Transition from Homogeneous to Localized Deformation in Nanoporous Gold

Ling-Zhi Liu,[1] Ye-Yuan Zhang,[1,2] Hui Xie,[1] and Hai-Jun Jin[1,*]
[1]Shenyang National Laboratory for Materials Science, Institute of Metal Research, Chinese Academy of Sciences, 110016 Shenyang, China
[2]School of Materials Science and Engineering, University of Science and Technology of China, 110016 Shenyang, China

(Received 29 March 2021; accepted 16 July 2021; published 24 August 2021)

We report a transition from homogeneous deformation to localized densification for nanoporous gold (NPG) under compression, with its solid fraction (φ) increasing to above $\sim 1/3$. Results obtained herein suggest that this transition is inverted compared to that of conventional porous materials. Consequently, under compression, the low-density NPGs with $\varphi < 1/3$ showed evident strain hardening, whereas a stress plateau was observed for high-density NPGs with $\varphi > 1/3$, which is contrary to the established notions for conventional porous materials. The ligament pinch-offs and bending-dominated structures are responsible for the homogeneous deformation of low-density NPGs. For high-density NPGs, the compression- or tension-dominated structure enables the collective strain bursts in nanoligaments, resulting in localized densification and stress plateau in their compression curves. In addition to the nanosize effect, the surface-diffusion-mediated topology evolution and the large-scale crystal-lattice coherency arising from the large grain size are also decisive to the mechanical response of dealloyed NPGs, which might be universal for self-organized nanonetwork materials.

DOI: 10.1103/PhysRevLett.127.095501

For conventional porous materials under compression, yielding is usually followed by a plateau region of constant stress in their stress-strain curves [1,2]. This stress plateau is associated with an inhomogeneous deformation, which proceeds by the formation and propagation of localized densification bands [3–5] and occurs typically in porous materials with a relative density (or solid fraction, φ) below 0.30 [6,7]. As an emerging nanomaterial, nanoporous (NP) metals [8–15] prepared by dealloying [16–18] are much stronger than conventional porous materials because of the "smaller is stronger" effect [19,20]. However, previous studies have revealed that NP metals, particularly nanoporous gold (NPG), deformed homogeneously under compression [21]. Their flow stress also increased steadily with increasing strain [10,13,14,22–25], showing no stress plateau. In one case [26], a plateaulike feature was observed in the compression of micron pillars machined from NPG with $\varphi = 0.30$, which was not confirmed in macroscopic NPGs with similar φ [27–29]. The relative density of previous NPGs is typically above 0.25 [12,14,30], and it even exceeds 0.30. According to the notions established in conventional porous materials, the homogeneous deformation and the lack of stress plateau in compression may be attributed to the high relative density of NPGs.

In this study, we report that a stress plateau was achieved in the compression of NPGs by further increasing but not decreasing the relative density. This phenomenon is associated with a transition from homogeneous to localized deformation in NPGs as φ increases to above $\sim 1/3$, which is inverted compared with that of conventional porous materials.

Figures 1(a)–1(c) show typical scanning electron microscopy (SEM) images of NPG-25, NPG-30, and NPG-35, which were prepared by dealloying $Au_{25}Ag_{75}$, $Au_{30}Ag_{70}$, and $Au_{35}Ag_{65}$, respectively. These NPGs, which were treated by a same postdealloying potential sweeping procedure (see Supplemental Material [31]), exhibit

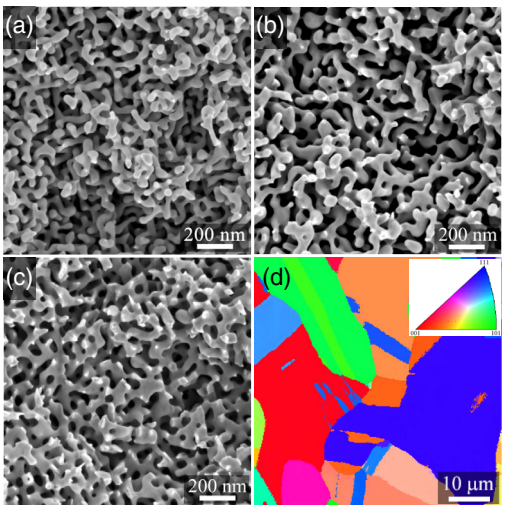

FIG. 1. Microstructure of NPG samples. Typical SEM images of (a) NPG-25, (b) NPG-30, and (c) NPG-35. (d) Electron backscatter diffraction (EBSD) orientation map of NPG-35 showing large grain sizes inherited from the precursor alloy.

TABLE I. Relative density (φ), ligament size (L), yield strength (σ_Y), and plastic Poisson's ratio (ν_P) of NPG samples.

Sample	φ	L (nm)	σ_Y (MPa)	ν_P
NPG-25	0.27 ± 0.01	32 ± 7	7.4	0.084 ± 0.024
NPG-30	0.31 ± 0.01	37 ± 8	23.4	0.075 ± 0.021
NPG-35	0.36 ± 0.01	37 ± 10	79.6	0.120 ± 0.042

uniform structures of similar ligament size (32–37 nm) but different relative densities, as summarized in Table I. The relative density of NPG is determined from the Au content in precursor alloy, the residual Ag content in obtained NPGs (<2 at.%), and the overall volume shrinkage during dealloying and processing (see Supplemental Material [31]). The standard deviation of the obtained φ data was within 0.01.

These NPGs exhibit large grain sizes inherited from their precursor alloys [21,32]. Figure 1(d) shows a grain size of ~30 μm (for NPG-35), which is 3 orders of magnitude larger than the ligament size. In other words, each grain is a single-crystal NPG containing $\sim 10^9$ Au ligaments. In each grain, although the network structure is random and the morphology of each ligament is different, the crystal structure and crystal orientation are identical for all the ligaments. Such a large-scale crystal-lattice coherency of NPG is not present in conventional porous materials, whose grain size is usually no larger than the ligament (strut) size.

Compression tests showed that the yield strength increased with increasing φ, from ~7 MPa of NPG-25 with $\varphi = 0.27$ to ~80 MPa of NPG-35 with $\varphi = 0.36$, as shown in Fig. 2(a). For both NPG-25 and NPG-30, the flow stress increases with increasing compression strain, which is consistent with the previous reports [21,29]. However, the flow stress of NPG-35 remained constant up to a strain of ~0.20, showing a well-defined plateau region that has not been observed in dealloyed NP metals [33,34]. This is the opposite of that observed in conventional porous materials, wherein the stress plateau is present and more evident at lower relative densities [6] [see the inset in Fig. 2(a)].

The strain-hardening rate (θ) was quantified as $\theta = d\sigma_f/d\varepsilon$, where σ_f and ε are the flow stress and engineering strain, respectively. The strain-hardening rate normalized by the flow stress, θ/σ_f, is plotted in Fig. 2(b) as a function of the strain, showing the different strain-hardening behaviors of different samples. As summarized in Fig. 2(c), the mean values of θ/σ_f measured at the early stage of compression ($\varepsilon = 0.05$–0.20) decreased systematically with increasing φ and approached zero at approximately $\varphi = 0.36$.

Thermal annealing can increase the ligament size of high-density NPG such as NPG-35, while its relative density remains almost unchanged [35]. Figure 2(d) shows that the stress plateau in the compression curves and, thus,

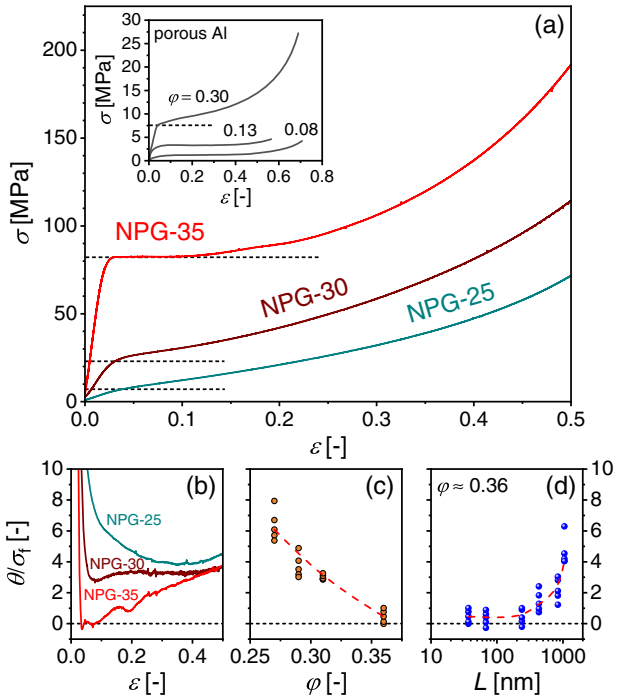

FIG. 2. Uniaxial compression behavior of NPG samples. (a) Engineering stress-strain ($\sigma - \varepsilon$) curves of NPGs at a strain rate of 10^{-4} s^{-1}. The inset shows the typical data of conventional porous aluminum (adapted from Ref. [2] with permission). The horizontal dotted lines indicate the level of yield stress for each sample. (b) Variation in normalized strain-hardening rate (θ/σ_f) with strain for different NPGs. (c) Variation in θ/σ_f at small strains ($\varepsilon = 0.07, 0.09, 0.11, 0.13$, and 0.15) with relative density. The ligament sizes of NPGs tested in (a)–(c) are between 30–40 nm (see Table I). (d) Variation in θ/σ_f (at small strains) with ligament size for NPG-35.

the near-zero θ/σ_f value of NPG-35 can be maintained after annealing, as long as the ligament size L is below 200 nm. Further coarsening resulted in a substantial increase in θ/σ_f with increasing L, showing the evolution of NPGs toward conventional porous materials (with positive θ/σ_f values at this relative density) during coarsening.

The decrease in θ/σ_f with increasing relative density of NPGs ($L < 200$ nm) is correlated with a transition from homogeneous to localized deformation in compression, as shown in Fig. 3. Consecutive optical images of compressed NPG samples clearly show that the deformation was uniform in low-density NPGs, such as NPG-25 [Fig. 3(a)], which agrees with the previous reports [14,21,23,24]. However, the deformation of NPG-35 was nonuniform, which was due to the propagation of the localized deformation, as shown in Fig. 3(b). Measurements of the local strain along the compression axis confirmed that the deformation was homogeneous in NPG-25 [Fig. 3(c)] and localized in NPG-35 [Fig. 3(d)] during the early stages of compression. The direction of this

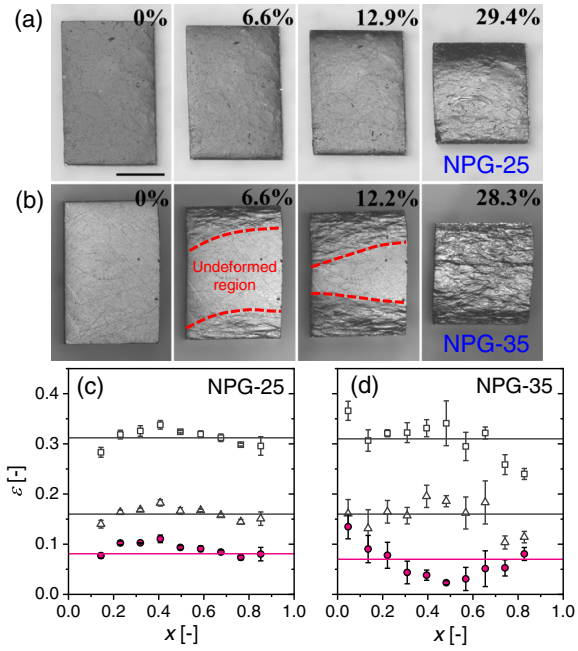

FIG. 3. Deformation of NPG under compression. Consecutive optical images of (a) NPG-25 and (b) NPG-35 samples compressed to different strains. The scale bar is 0.5 mm. The dashed lines in (b) indicate the boundaries between the deformed and undeformed regions. Local plastic strain was measured along the compression axis for (c) NPG-25 and (d) NPG-35 at different strains. Solid lines indicate the overall plastic strain for each set of data. The distance to one end of the sample was normalized by the length of the sample.

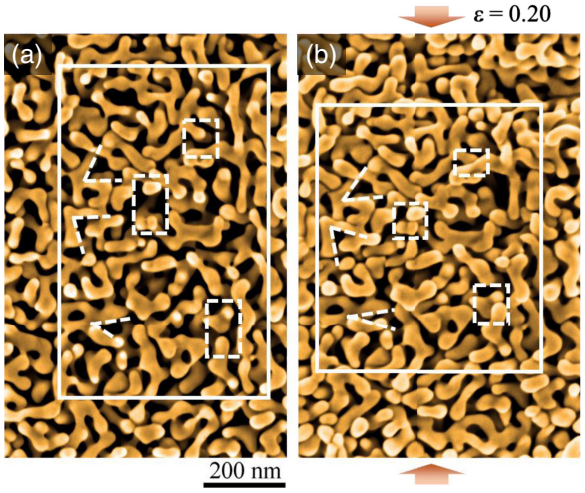

FIG. 4. SEM observation of the same area on the surface of NPG-25 (a) before and (b) after compression ($\varepsilon = 0.20$). The rectangles of the solid line indicate the same area before and after compression. The bending and touching of ligaments are also indicated for the compressed sample. Color was added to enhance the contrast of the labels.

transition was inverted compared with that observed in conventional porous materials.

For low-density NPGs such as NPG-25, SEM images before and after compression confirm that the deformation is uniform down to the scale of ligament size, as shown in Fig. 4. The plastic strain in this region (enclosed by a solid white box) agrees well with the macroscopic strain of this sample. The bending of ligaments, which was frequently observed after compression, might be the dominant deformation mechanism of this sample. Figure 4 also shows the torsion or rotation of ligaments about the out-of-plane axis, which likely resulted from the fact that ligaments on the surface were less constrained compared with those in the interior of the sample.

For NPG-35 under compression, the plastic deformation was inhomogeneous at both macroscopic [see Fig. 3(b)] and microscopic scales (Fig. 5). In the NPG-35 compressed to 0.10 (in the plateau region), we observed large-population bandlike deformation structures in the deformed region, particularly in the transition zone between deformed and undeformed regions. As shown in Fig. 5(a), these deformation bands (DBs) are 1–3 μm thick, and, sometimes, two sets of parallel DBs cross each other in one grain. While most DBs terminate at grain boundaries, some can extend deep into adjacent grains. EBSD analysis shows that these DBs do not lie on the $\{111\}$ planes [Fig. 5(b)], which are favorable slip planes of Au. Figures 5(c) and 5(d) confirm that, at microscopic scale, severe deformation can be easily identified within each DB [Fig. 5(c)], while the matrix (or the region between two DBs) remains intact and undeformed [Fig. 5(d)].

The detailed structure of DB in NPG-35 is presented in Fig. 5(e), showing high-population narrow slip traces aligned along specific directions. In this DB, two sets of slip traces or lines can be easily identified, which are parallel to the intersection lines of the $\{111\}$ planes with the sample surface, according to the crystallographic analysis in this region (see the inset; it is a single crystal in the imaged region). This confirms that these slip traces were formed by the glide of dislocations on the $\{111\}$ planes. Interestingly, slip traces were observed not only in thin ligaments but also in thick ligaments and nodes.

In short, the deformation of low-density NPGs with φ below $\sim 1/3$ is homogeneous and dominated by ligament bending, and the deformation of high-density NPGs with φ exceeding $\sim 1/3$ proceeds by the propagation of localized DBs, wherein the ligaments deform by shear or slip. Different deformation behaviors have resulted in distinct plastic responses, i.e., evident strain hardening for low-density NPGs and a stress plateau for high-density NPGs in their compression stress-strain curves, although the overall elastic modulus increases with increasing compression for both types of NPG (see Fig. S2 in Supplemental Material [31]), in accordance with earlier work on porous solids [36,37].

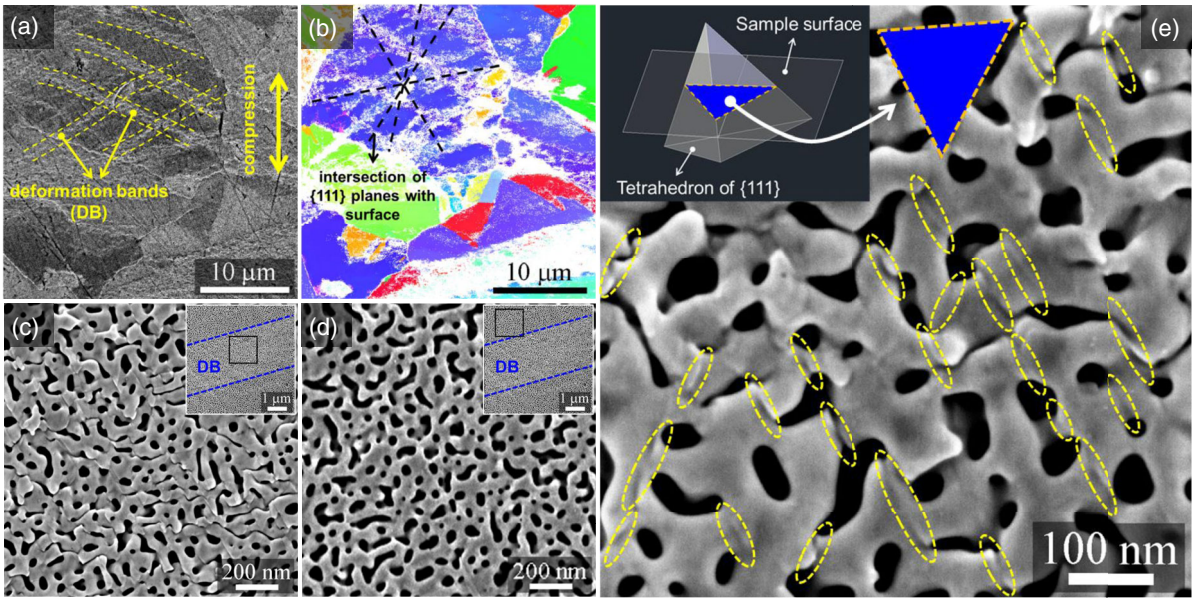

FIG. 5. Microstructure of NPG-35 compressed to $\varepsilon = 0.10$, in an area between deformed and undeformed regions. (a) Backscatter electron SEM image and (b) EBSD map of the same location of deformed NPG-35. The dashed lines in (b) represent the intersection lines of the $\{111\}$ planes with the sample surface in this grain. SEM images taken in a region (c) within or (d) out of a DB, as indicated in the inset. (e) High-magnification SEM image of a DB, where the slip traces are indicated by dotted ellipses. Inset: intersection lines of $\{111\}$ planes with the sample surface in this area.

The slip of ligaments observed in compressed NPG-35 suggests that the ligaments therein might undergo a compression or tension load, unlike the bending of ligaments observed in NPG-25. Indeed, molecular dynamics simulations have revealed an *elastic* bending-to-compression or -tension transition in the structure of NPGs (gyroid structure) as φ increases to above 0.35 [38]. Atomistic simulation [39] also revealed an evidently decreased density of (geometrically necessary) dislocations in NPGs with $\varphi > 0.35$ after deformation, indicating a *plastic* bending-to-compression or -tension transition at a similar φ.

Furthermore, driven by the Plateau-Rayleigh instability, gold ligaments pinch-off via surface diffusion as φ decreases to below $\sim 1/3$, giving rise to large-population dangling ligaments in low-density NPGs [14,23,40–42]. This phenomenon has resulted in anomalous sintering [35] and a severe deviation in strength [23,24,43,44] and elastic modulus [14,23,40,42,44,45] from theoretical predictions [1], in NPGs with $\varphi < 1/3$. The Plateau-Rayleigh instability could even lead to a percolation-to-cluster transition at around $\varphi = 0.159$, which sets a lower limit for φ of monolithic NPG self-organized in dealloying [42,46]. The capillarity-driven topology evolution might (at least partially) account for the bending-to-compression or -tension transition and, eventually, the changes in the mechanical response of NPGs, as φ crosses $\sim 1/3$.

In *low-density* NPGs with $\varphi < 1/3$, the presence of large-population dangling ligaments and the bending-dominated structure might account for their homogeneous deformation and the absence of a stress plateau under compression. For conventional foams, the stress plateau under compression is usually associated with a mechanism of plastic or elastic instability (such as buckling or crushing of ligaments [6,7]), which is lacking in low-density NPGs. When a low-density NPG is under compression, the reconnection or coalescence of dangling ligaments results in local hardening or stiffening. Furthermore, the plastic bending of ligaments introduces a large strain gradient and, thus, large-population geometrically necessary dislocations, which further strengthen the ligaments [39,47]. These local strain-hardening mechanisms might suppress strain localization and trigger the homogeneous deformation of low-density NPGs (such as NPG-25) under compression.

For *high-density* NPGs with $\varphi > 1/3$, the slip traces observed in compressed samples indicate that the strain burst of ligaments might act as a mechanism of plastic instability, which is responsible for the inhomogeneous deformation and stress plateau of high-density NPGs. Discrete strain bursts, which have been widely observed in the compression of nano- or submicron-scale single-crystal pillars [48–52], are associated with dislocation avalanches (i.e., the sudden emission or gliding of a large number of dislocations in a narrow region). Such a strain burst is prevalent in the source-controlled plasticity, which typically occurs in pillars with diameters below 150 nm [53]. This scenario is consistent with the observations shown in Fig. 2(d); θ/σ_f of coarsened NPG-35 increases gradually as the ligament size increases to above ~200 nm.

We emphasize that, in addition to the small ligament size and compression- or tension-dominated NP structure, the large-scale crystal-lattice coherency is also essential to the stress plateau in NPGs. Dislocation slip avalanches in one ligament would impose a shear stress in the network and facilitate strain bursts of adjacent ligaments if they have identical crystal orientations. The collective strain bursts result in the formation and propagation of DBs and, eventually, in the inhomogeneous deformation of NPG-35 and the stress plateau in its compression stress-strain curves. This scenario is supported by the absence of a stress plateau in the compression of nanocrystalline NPGs [54] (see Fig. S3 in Supplemental Material [31]), wherein the grain size is no larger than the ligament size (and nanocrystalline NP Al with native oxide shell [55]), although their solid fractions are well beyond $1/3$.

Previous simulations also showed a stress plateau in the compression of NPGs [56–59]. However, this phenomenon was observed in both high-density and low-density NPGs without DBs or localized densification, which is inconsistent with our experimental observations. The discrepancy between the experiment and simulation may result from the fact that the simulated samples were much smaller than those used in this study, and they were even smaller than the characteristic size (thickness) of the DBs observed in deformed NPGs. This also raises the question of whether the mechanical response and deformation behavior of NPGs will be maintained as the sample size decreases to below DB thickness, particularly for coarse-grained high-density NPGs. This issue may be clarified in the future by conducting submicron pillar compression tests on high-density NPGs.

In summary, we report an unexpected transition from homogeneous to localized deformation for NPGs under compression, as φ increases to above $\sim 1/3$, owing to the combined effects of small ligaments, topology structure, and large-scale crystal-lattice coherency. The observations in this study for dealloyed NPGs, which are distinct to that of conventional porous materials, might be universal for self-organized nanonetwork materials whose topology structures are shaped by capillarity-driven surface diffusion. Other methods may produce NP materials with conventional-porous-material-like deformation behavior; however, such structure will be unstable and evolve toward a NPG-like structure or fall apart into nanoparticles (if not densify spontaneously [60,61]) when $\varphi < 0.16$ [42], if surface diffusion is not too slow.

Financial support from the National Key R&D Program of China (Grant No. 2017YFA0204401) and the National Natural Science Foundation of China (Grants No. 51971218 and No. 52001316) is gratefully acknowledged.

*Corresponding author.
hjjin@imr.ac.cn

[1] L. J. Gibson and M. F. Ashby, *Cellular Solids: Structure and Properties*, 2nd ed., Cambridge Solid State Science Series (Cambridge University Press, Cambridge, England, 1997).
[2] M. F. Ashby, T. Evans, N. A. Fleck, J. Hutchinson, H. Wadley, and L. Gibson, *Metal Foams: A Design Guide* (Elsevier, New York, 2000).
[3] M. F. Vaz and M. Fortes, Characterization of deformation bands in the compression of cellular materials, J. Mater. Sci. Lett. **12**, 1408 (1993).
[4] W.-Y. Jang and S. Kyriakides, On the crushing of aluminum open-cell foams: Part I. Experiments, Int. J. Solids Struct. **46**, 617 (2009).
[5] L. J. Gibson, Mechanical behavior of metallic foams, Annu. Rev. Mater. Sci. **30**, 191 (2000).
[6] M. F. Ashby and R. M. Medalist, The mechanical properties of cellular solids, Metall. Trans. A **14**, 1755 (1983).
[7] S. Maiti, L. Gibson, and M. Ashby, Deformation and energy absorption diagrams for cellular solids, Acta Metall. **32**, 1963 (1984).
[8] J. Biener, A. M. Hodge, A. V. Hamza, L. M. Hsiung, and J. H. Satcher, Nanoporous Au: A high yield strength material, J. Appl. Phys. **97**, 024301 (2005).
[9] A. Hodge, J. Biener, J. Hayes, P. Bythrow, C. Volkert, and A. Hamza, Scaling equation for yield strength of nanoporous open-cell foams, Acta Mater. **55**, 1343 (2007).
[10] C. A. Volkert, E. T. Lilleodden, D. Kramer, and J. Weissmüller, Approaching the theoretical strength in nanoporous Au, Appl. Phys. Lett. **89**, 061920 (2006).
[11] X.-L. Ye and H.-J. Jin, Corrosion-induced strengthening: Development of high-strength nanoporous metals, Adv. Eng. Mater. **18**, 1050 (2016).
[12] N. Badwe, X. Chen, and K. Sieradzki, Mechanical properties of nanoporous gold in tension, Acta Mater. **129**, 251 (2017).
[13] L. Lührs and J. Weissmüller, Nanoporous copper-nickel: Macroscopic bodies of a strong and deformable nanoporous base metal by dealloying, Scr. Mater. **155**, 119 (2018).
[14] H.-J. Jin, J. Weissmüller, and D. Farkas, Mechanical response of nanoporous metals: A story of size, surface stress, and severed struts, MRS Bull. **43**, 35 (2018).
[15] H. Kashani and M. Chen, Flaw-free nanoporous Ni for tensile properties, Acta Mater. **166**, 402 (2019).
[16] J. Erlebacher, M. J. Aziz, A. Karma, N. Dimitrov, and K. Sieradzki, Evolution of nanoporosity in dealloying, Nature (London) **410**, 450 (2001).
[17] J. Weissmüller, R. C. Newman, H.-J. Jin, A. M. Hodge, and J. W. Kysar, Nanoporous metals by alloy corrosion: Formation and mechanical properties, MRS Bull. **34**, 577 (2009).
[18] I. McCue, E. Benn, B. Gaskey, and J. Erlebacher, Dealloying and dealloyed materials, Annu. Rev. Mater. Res. **46**, 263 (2016).
[19] M. D. Uchic, Sample dimensions influence strength and crystal plasticity, Science **305**, 986 (2004).

[20] J. R. Greer, W. C. Oliver, and W. D. Nix, Size dependence of mechanical properties of gold at the micron scale in the absence of strain gradients, Acta Mater. **53**, 1821 (2005).
[21] H.-J. Jin, L. Kurmanaeva, J. Schmauch, H. Rösner, Y. Ivanisenko, and J. Weissmüller, Deforming nanoporous metal: Role of lattice coherency, Acta Mater. **57**, 2665 (2009).
[22] T. J. Balk, C. Eberl, Y. Sun, K. J. Hemker, and D. S. Gianola, Tensile and compressive microspecimen testing of bulk nanoporous gold, JOM **61**, 26 (2009).
[23] L.-Z. Liu, X.-L. Ye, and H.-J. Jin, Interpreting anomalous low-strength and low-stiffness of nanoporous gold: Quantification of network connectivity, Acta Mater. **118**, 77 (2016).
[24] N. Mameka, K. Wang, J. Markmann, E. T. Lilleodden, and J. Weissmüller, Nanoporous gold—testing macro-scale samples to probe small-scale mechanical behavior, Mater. Res. Lett. **4**, 27 (2015).
[25] B.-N. D. Ngô, A. Stukowski, N. Mameka, J. Markmann, K. Albe, and J. Weissmüller, Anomalous compliance and early yielding of nanoporous gold, Acta Mater. **93**, 144 (2015).
[26] J. Biener, A. M. Hodge, J. R. Hayes, C. A. Volkert, L. A. Zepeda-Ruiz, A. V. Hamza, and F. F. Abraham, Size effects on the mechanical behavior of nanoporous Au, Nano Lett. **6**, 2379 (2006).
[27] N. J. Briot, T. Kennerknecht, C. Eberl, and T. J. Balk, Mechanical properties of bulk single crystalline nanoporous gold investigated by millimetre-scale tension and compression testing, Philos. Mag. **94**, 847 (2014).
[28] M. Bürckert, N. J. Briot, and T. J. Balk, Uniaxial compression testing of bulk nanoporous gold, Philos. Mag. **97**, 1157 (2017).
[29] H. Jeon, S. Lee, and J.-Y. Kim, Tension-compression asymmetry in plasticity of nanoporous gold, Acta Mater. **199**, 340 (2020).
[30] N. J. Briot and T. J. Balk, Developing scaling relations for the yield strength of nanoporous gold, Philos. Mag. **95**, 2955 (2015).
[31] See Supplemental Material at http://link.aps.org/supplemental/10.1103/PhysRevLett.127.095501 for experimental details and Figs. S1–S3.
[32] S. V. Petegem, S. Brandstetter, R. Maass, A. M. Hodge, B. S. El-Dasher, J. Biener, B. Schmitt, C. Borca, and H. V. Swygenhoven, On the microstructure of nanoporous gold: An x-ray diffraction study, Nano Lett. **9**, 1158 (2009).
[33] This observation is confirmed in a preproof manuscript published online by Zandersons *et al.* [34] recently. The focus of Zandersons *et al.*'s work was on the yield strength but not the deformation behavior reported in this study.
[34] B. Zandersons, L. Lührs, Y. Li, and J. Weissmüller, On factors defining the mechanical behavior of nanoporous gold, Acta Mater. **215**, 116979 (2021).
[35] H. Xie, H. Guan, L.-Z. Liu, and H.-J. Jin, A critical relative density and a break-and-reconnect model for annealing-induced densification in nanoporous gold, Acta Mater. **209**, 116806 (2021).
[36] A. Papathanassiou, Contribution of the pressure variation of the porosity to the activation volume evaluation from ionic conductivity measurements under pressure, J. Phys. Chem. Solids **58**, 2107 (1997).
[37] A. N. Papathanassiou, Evaluation of the activation volume from ionic conductivity measurements under pressure in porous materials, Phys. Rev. B **58**, 16038 (1998).
[38] H. Liu and N. Abdolrahim, A modified scaling law for stiffness of nanoporous materials based on gyroid cell model, Int. J. Mech. Sci. **166**, 105223 (2020).
[39] N. Beets and D. Farkas, Mechanical response of Au foams of varying porosity from atomistic simulations, JOM **70**, 2185 (2018).
[40] L.-Z. Liu and H.-J. Jin, Scaling equation for the elastic modulus of nanoporous gold with "fixed" network connectivity, Appl. Phys. Lett. **110**, 211902 (2017).
[41] Y. Li, B.-N. Dinh Ngô, J. Markmann, and J. Weissmüller, Topology evolution during coarsening of nanoscale metal network structures, Phys. Rev. Mater. **3**, 076001 (2019).
[42] C. Soyarslan, S. Bargmann, M. Pradas, and J. Weissmüller, 3d stochastic bicontinuous microstructures: Generation, topology and elasticity, Acta Mater. **149**, 326 (2018).
[43] H.-J. Jin, X.-L. Wang, S. Parida, K. Wang, M. Seo, and J. Weissmüller, Nanoporous Au-Pt alloys as large strain electrochemical actuators, Nano Lett. **10**, 187 (2010).
[44] K. Mangipudi, E. Epler, and C. Volkert, Morphological similarity and structure-dependent scaling laws of nanoporous gold from different synthesis methods, Acta Mater. **140**, 337 (2017).
[45] N. Mameka, J. Markmann, H.-J. Jin, and J. Weissmüller, Electrical stiffness modulation—confirming the impact of surface excess elasticity on the mechanics of nanomaterials, Acta Mater. **76**, 272 (2014).
[46] S. Shi, Y. Li, B.-N. Ngo-Dinh, J. Markmann, and J. Weissmüller, Scaling behavior of stiffness and strength of hierarchical network nanomaterials, Science **371**, 1026 (2021).
[47] R. Dou and B. Derby, Deformation mechanisms in gold nanowires and nanoporous gold, Philos. Mag. **91**, 1070 (2011).
[48] H. Tang, K. W. Schwarz, and H. D. Espinosa, Dislocation-Source Shutdown and the Plastic Behavior of Single-Crystal Micropillars, Phys. Rev. Lett. **100**, 185503 (2008).
[49] C. A. Volkert and E. T. Lilleodden, Size effects in the deformation of sub-micron Au columns, Philos. Mag. **86**, 5567 (2006).
[50] A. T. Jennings, M. J. Burek, and J. R. Greer, Microstructure versus Size: Mechanical Properties of Electroplated Single Crystalline Cu Nanopillars, Phys. Rev. Lett. **104**, 135503 (2010).
[51] X. Ni, H. Zhang, D. B. Liarte, L. W. McFaul, K. A. Dahmen, J. P. Sethna, and J. R. Greer, Yield Precursor Dislocation Avalanches in Small Crystals: The Irreversibility Transition, Phys. Rev. Lett. **123**, 035501 (2019).
[52] J. R. Greer and J. T. D. Hosson, Plasticity in small-sized metallic systems: Intrinsic versus extrinsic size effect, Prog. Mater. Sci. **56**, 654 (2011).
[53] A. T. Jennings, J. Li, and J. R. Greer, Emergence of strain-rate sensitivity in Cu nanopillars: Transition from dislocation multiplication to dislocation nucleation, Acta Mater. **59**, 5627 (2011).

[54] Y.-Y. Zhang, H. Xie, L.-Z. Liu, and H.-J. Jin, Surface Triple Junctions Govern the Strength of a Nanoscale Solid, Phys. Rev. Lett. **126**, 235501 (2021).

[55] W. Yang, Z.-P. Luo, W.-K. Bao, H. Xie, Z.-S. You, and H.-J. Jin, Light, strong, and stable nanoporous aluminum with native oxide shell, Sci. Adv. **7**, eabb9471 (2021).

[56] C. J. Ruestes, D. Farkas, A. Caro, and E. M. Bringa, Hardening under compression in Au foams, Acta Mater. **108**, 1 (2016).

[57] N. Beets, D. Farkas, and K. Albe, The mechanical response of nanoporous gold and silver foams with varying composition and surface segregation, Acta Mater. **203**, 116445 (2021).

[58] M. H. Saffarini, G. Z. Voyiadjis, C. J. Ruestes, and M. Yaghoobi, Ligament size dependency of strain hardening and ductility in nanoporous gold, Comput. Mater. Sci. **186**, 109920 (2021).

[59] S. Mathesan and D. Mordehai, On the yielding and densification of nanoporous Au nanopillars in molecular dynamics simulations, Comput. Mater. Sci. **191**, 110307 (2021).

[60] S. Parida, D. Kramer, C. A. Volkert, H. Rösner, J. Erlebacher, and J. Weissmüller, Volume Change During the Formation of Nanoporous Gold by Dealloying, Phys. Rev. Lett. **97**, 035504 (2006).

[61] X.-L. Ye, N. Lu, X.-J. Li, K. Du, J. Tan, and H.-J. Jin, Primary and secondary dealloying of Au(Pt)-Ag: Structural and compositional evolutions, and volume shrinkage, J. Electrochem. Soc. **161**, C517 (2014).